# Structural Properties of Ferroelectric heterostructures using Coherent Bragg Rod Analysis

Kyeong Jun Lee[1†], Yeong Jae Shin[2,3,4†], Taeyang Choi[1], Tae Won Noh[2,3], Hua Zhou[5], Seo Hyoung Chang[1*]

[1]Department of Physics, Chung-Ang University, Seoul 156-756, Republic of Korea
[2]Center for Correlated Electron Systems, Institute for Basic Science (IBS), Seoul 08826, Republic of Korea
[3]Department of Physics and Astronomy, Seoul National University, Seoul 08826, Republic of Korea
[4]Department of Applied Physics, Yale University, New Haven, Connecticut 06511, United States of America
[5]X-Ray Science Division, Advanced Photon Source, Argonne National Laboratory, Argonne, IL 60439

e-mail: cshyoung@cau.ac.kr

**We investigated the crystal structure of $SrRuO_3$/$BaTiO_3$/$SrRuO_3$ (SRO/BTO/SRO) heterostructures grown on $SrTiO_3$ (001) substrate by using X-ray scattering. The interface structure of SRO/BTO/SRO heterostructures can make the critical thickness of ferroelectric BTO films decreased down into 3.5 unit cells. Owing to weak intensity of ultrathin films, lab source-based X-ray measurement can hardly determine the atomic arrangement of the heterostructures and their lattice parameters. To resolve the detailed structure of the heterostructures, we introduced synchrotron-based X-ray scattering techniques combined with coherent Bragg rod analysis (COBRA). Based on the electron density profiles of the heterostructures from COBRA results, we were able to obtain their detailed crystal structural information, e.g., the lattice parameters and atomic arrangements of the SRO/BTO/SRO heterostructures.**

Keywords: Ferroelectricity, $BaTiO_3$, $SrRuO_3$, Coherent Bragg Rod Analysis, X-ray scattering

## 1. Introduction

Oxide heterostructures are exciting model systems for exploring emergent physical properties, such as two-dimensional electron gas, metal-insulator transition, superconductivity, and ferroelectricity.[1-8] Recent advances of atomic-level film fabrication can lead to achieve the physical properties that don't exist in nature[4, 9-11]. Using ultrathin ferroelectric oxide heterostructures, many researchers have great attention on the thickness limit of nanoscale devices retaining the ferroelectricity, so called critical thickness. Deeper understanding on the critical thickness of ferroelectric materials provides the route to miniaturize the nanoscale functional devices and to achieve high-density nonvolatile random access memory.

To engineer oxide heterostructures with the atomic control for the critical thickness studies, the $SrRuO_3$/$BaTiO_3$/$SrRuO_3$ (SRO/BTO/SRO) heterostructure is an interesting model system, as shown in Figure 1. Because recent study on the system found that the critical thickness of ferroelectric BTO film was quite low, i.e., 3.5 unit cells (u.c.) of BTO layer having three BaO layers and four $TiO_2$ layers.[12] However, it was very sensitive to the interface structure between ferroelectric BTO layer and the SRO electrodes. For instance, the symmetric interface such as the same SrO-$TiO_2$ terminations in the SRO/BTO/SRO heterostructures could reduce the pinned dipoles and enhance the stability of ferroelectric polarization compared with the different mixed terminations, e.g., $RuO_2$-BaO and SrO-$TiO_2$. It leads to preserve the ferroelectricity in the ultrathin limit. To elucidate the relation between the structure and ferroelectricity, the key characterization is the direct experimental verification of the atomic arrangement of oxide heterostructures.

Here, we introduce coherent Bragg rod analysis (COBRA) technique based on surface X-ray scattering, which is a phase-retrieval X-ray diffraction approach.[13-15] It is still challengeable to nondestructively determine the structure of ultrathin films with sub-Angstrom resolution. For instance, transmission electron microscopy (TEM) usually needs special sample treatments and easily perturbs the ferroelectric polarization or samples. Lab source-based X-ray diffraction hardly observes the structure of ultrathin films due to the weak intensity. Synchrotron-based X-ray scattering combined with COBRA can non-destructively obtain the electron density map and detailed crystal structure by

Fourier transformation of calculated complex scattering factors (CSF).[14] The COBRA method also can achieve three-dimensional electron density map and reconstruct the following crystal structure.

In this paper, we visualized the atomic-level three-dimensional structure of the $SrRuO_3$/$BaTiO_3$ /$SrRuO_3$ (SRO/BTO/SRO) heterostructures grown on $SrTiO_3$ (STO)(001) by using X-ray scattering combined with COBRA technique. We systematically measured the crystal truncation rods of SRO/BTO/SRO heterostructures in three-dimensional reciprocal space and analyzed their electron density map using COBRA. We visualized their atomic arrangement of the heterostructures, specifically (200) plane and (001) plane. We also plotted the electron density along the z-direction at (0 0), (0.5 0.5), and (0 0.5) position for A-site ion, B-site ion, and oxygen, respectively. From the calculated electron density maps, we were able to determine the individual lattice parameters of three layers in the heterostructure, leading to a relation between the stability of ferroelectric polarization and the critical thickness.

## 2. Experimental methods

The SRO/BTO/SRO heterostructures were epitaxially grown on $TiO_2$-terminated $SrTiO_3$ (STO)(001) substrates using the pulsed laser deposition (PLD) technique. The SRO and BTO ceramic targets were ablated with a KrF excimer laser (248 nm, COMPex pro, Coherent). For the COBRA, the total thicknesses of the heterostructures were 10 – 15 u.c.. Detailed growth conditions were described elsewhere.[12] The x-ray scattering measurements were carried out at Sector 12-ID-D at Advanced Photon Source, Argonne National Laboratory and at Sector 5A at Pohang Accelerator Laboratory. The two-dimensional images of the crystal truncation rods were measured with an area detector (Dectris PILATUS 100K) under X-ray photon energy of 23.5 keV or 16 keV. All specular and off-specular crystal truncation rods were analyzed using the COBRA method.

## 3. Results and discussions

Figure 1 shows the ferroelectric BTO film (3.5 u.c.) sandwiched by top and bottom SRO layers (3 u.c.) grown on the STO (001) substrate. The building blocks are $ABO_3$ perovskite structure, consisting of AO and $BO_2$ layer. The crystal structure of BTO at room temperature is tetragonal with *P4/mmm* symmetry.[16] The structures of SRO and STO are orthorhombic and cubic, respectively at room temperature. The lattice parameters of perovskite STO are a = b = c = 3.905 Å.[17] The in-plane lattice parameters of fully strained ultrathin SRO and BTO films are also identical with 3.905 Å, confirmed by X-ray scattering measurements. Based on the previous study, manipulating the oxygen partial pressure during the BTO growth efficiently were able to achieve a uniform SrO-$TiO_2$ termination rather than BaO-$RuO_2$ termination at the SRO/BTO interface due to the thermodynamic stability of the BTO. We fabricated the SRO(3 u.c.)/BTO(3.5 u.c.)/SRO(u.c.) heterostructure as a model system for COBRA via the termination engineering, i.e., the atomic-level control of stacking layer at the 0.5 u.c level.

To investigate the three-dimensional crystal structure of our system, we performed synchrotron-based X-ray scattering studies, as shown in Figure 2. Figure 2a displays the schematics of X-ray scattering measurements with two-dimensional area detector. From infinite periodic layers like STO single-crystal substrates, the scattered X-ray generates the diffraction pattern like delta function. These normal Bragg peaks of STO has very strong intensity and are easily detected by the lab source-based X-ray diffraction. However, the diffracted patterns from ultrathin films are usually very broad and weak intensity signal because of finite periodicity and are constructed along the normal lines in reciprocal space to the surface of the thin film. The intensity distributions of the diffraction along these lines are called as crystal truncation rods (CTRs).

The measured representative CTR data along (10L), (20L), (30L) of SRO/BTO/SRO heterostructures are presented in Fig. 2(b), 2(c), and 2(d), respectively. The measured CTR data has sharp Bragg peaks at each integer originating from the STO substrate and weak but clearly noticeable patterns from ultrathin films. To reconstruct the three-dimensional atomic level crystal structure using COBRA technique, we measured the complete data set with the consideration of symmetry-equivalency and resolution: e.g., (00L), (10L), (11L), (20L), (21L), (22L), (30L), (31L), (32L), (33L), (40L), (41L), and (42L). The index of plane (HKL) represents the STO cubic notation.

Our method is to efficiently find the proper electron densities of the system and the complex structure factors of our unknown structure.[13-15] The complex structure factors are calculated from the measured CTR data using Fourier transformation, directly connected to three-dimensional electron densities of the system. The complex structure factor $\mathcal{F}$ is described as

$$\mathcal{F}(\vec{q}) = \int_V \rho(\vec{r}) \cdot e^{i\vec{q}\cdot\vec{r}} d^3r \quad (1),$$

where $\vec{q}$ the position vector in reciprocal space, $\vec{r}$ is the position vector in real space, $\rho$ the electron density and the integral is over the volume of the sample. Firstly, using Eq. (1) these complex phase factor in the analysis was calculated from the initial model system having BTO film, SRO top/bottom layers, and STO substrates. The complex structure factor in Eg. (1) is the linear combination contributed from the reference and unknown structure related to the films, as following Eq. (2).

$$\mathcal{F}_{total} = \mathcal{F}_{ref} + \mathcal{F}_{unkown} \quad (2)$$

$$\rho(\vec{r}) = \int \mathcal{F}(\vec{q}) \mathrm{e}^{-i\vec{q}\cdot\vec{r}} d^3q \quad (3)$$

Note that the reference structure factor $\mathcal{F}_{ref}$ and different unknown structure factor $\mathcal{F}_{unknown}$ provides the sharp Bragg peaks and very weak signal in the CTR, as shown in Fig. 2. Secondly, we compared the calculated intensities with the experimental intensities. Using inverse Fourier Transformation like Eg. (3), the electron density can be calculated from the $\mathcal{F}$ to the real space. If acceptable, the result becomes the updated reference structure. Here, the $\mathcal{F}_{unknown}$ can be spatially distinguishable with the $\mathcal{F}_{ref}$ based on the simple assumption, so called the COBRA ansatz. The ansatz assumed that the $\mathcal{F}_{unknown}$ were slowly changed along the rod compare to the $\mathcal{F}_{ref}$. Therefore, the difference between the updated reference and the calculated electron density is converged quickly within small iterations.

As shown in Figure 3, our COBRA-based two-dimensional electron density cutting through planes clearly demonstrated that the number of BaO layers in the heterostructure was exactly three. The (200) plane in Fig. 2(a) shows the atomic-level stacking sequence, e.g., bottom SrO, BaO, and top SrO layers. In the electron density map, the intensity (or integrated electron density) at the specific position is correlated to the atom's total number of electrons. Then, it is quite reasonable that the intensity of Ba site (atomic number: 56) was higher than that of Sr site (atomic number: 38), as shown in Fig. 3(a). The intensity of O-site (atomic number: 8) was much weaker than the others. Furthermore, the COBRA-based electron density map contains three-dimensional crystal structure so we can certainly obtain the in-plane structure, as shown in Fig. 3(b). Here is a (001) plane through the Ti and O atoms near the BTO film region.

To get further insight on the detailed interface structure, we plotted one-dimensional electron density profiles along the z-direction at three different positions in $ABO_3$ perovskite structure: (0 0), (0.5 0.5), and (0.5 0) in Fig. 4 (a), (b), and (c), respectively. As mentioned before, we noticed the apparent three Ba layers sandwiched by Sr layers because of higher intensity of Ba than that of Sr. As shown in Fig. 4(b), we also verified that the numbers of Ti and Ru bottom (top) layers in the SRO/BTO/SRO heterostructures were four and three (three), respectively. Note that the atomic numbers of Ru and Ti are 44 and 22, respectively. Specifically, the interface structures near the bottom and top SRO electrodes exhibited the following stacking sequences: (bottom) $RuO_2$-SrO-$TiO_2$-1$^{st}$ BaO and (top) 3$^{rd}$ BaO-$TiO_2$-SrO-$RuO_2$. Using the COBRA method, we confirmed that the thickness of BTO film was 3.5 u.c. and the interface structure of the heterostructure was symmetric at the atomic-level.

Moreover, COBRA-calculated electron density profiles offered the lattice parameters of each individual SRO and BTO layers, as shown in Fig. 5. The atomic positions along the z-direction were extracted by fitting one Gaussian to each peak in the electron density profiles in Fig. 4. The lattice parameters were determined by the spacing between AO (or $BO_2$) layer and next nearest AO (or $BO_2$) layer. Although our initial reference model allowed to modulate the atomic positions of 7 u.c. STO substrate, the STO exhibited nearly quite similar lattice parameter of bulk STO, i.e., 3.905 Å. Due to the strain and coherent growth, the in-plane lattice of BTO layer was clamped with those of SRO (or STO) and the out-of-plane lattice parameters of BTO layers were around 4.08 Å. Intriguingly, the out-of-plane lattice parameters of SRO top and bottom electrodes were significantly altered by the BTO layers. Further investigation on the direction of polarization and octahedral rotation is needed.

## 4. Conclusion

In summary, we determined the atomic-level structural properties of the $SrRuO_3/BaTiO_3/SrRuO_3$ (SRO/BTO/SRO) heterostructures using Coherent Bragg Rod Analysis (COBRA) method. The COBRA based on crystal truncation rod (CTR) scans can visualize the three-dimensional atomic arrangement of the heterostructures. Then, we confirmed the BTO layer was 3.5 unit cells and the SRO/BTO/SRO) heterostructures exhibited the symmetric interface, which can enhance the ferroelectric stability. Furthermore, we were able to quantitatively define the positions of atoms and determine the individual lattice parameters of three layers in the heterostructure. COBRA method provides the huge potential and possibility to investigate the detailed structural and physical properties of the ultrathin films and oxide heterostructures.

**Acknowledgments**

The work of KJL is supported in part by the Chung-Ang University Graduate Research Scholarship in 2018.

**Figure Captions**

**Figure 1 |** Schematic of ferroelectric heterostructure model system. The atomic stacking of $SrRuO_3$(SRO, 3 unit cells (u.c.))/$BaTiO_3$ (BTO, 3.5 u.c.)/$SrRuO_3$ (SRO, 3 u.c.) films grown on $SrTiO_3$ (STO) substrate along the [001] direction.

**Figure 2 |** Crystal truncation rods (CTR) measurements of SRO/BTO/SRO heterostructures for coherent Bragg rod analysis (COBRA). (a) Schematics of Synchrotron-based X-ray scattering with area detector and measured three-dimensional reciprocal space represented by (H K L) of STO. Representative CTR data along (b) (10L), (c) (20L), and (c) (30L).

**Figure 3 |** Two-dimensional electron density maps obtained by COBRA. (a) (200) plane of SRO/BTO/SRO heterostructure demonstrating SrO and BaO stacking sequence. (b) (001) plane of the heterostructure, which can show $TiO_2$-site in the BTO layer.

**Figure 4 |** COBRA-calculated electron density profiles of the heterostructure at three sites in ABO3 perovskite structure along the z-direction: (a) A-site (Sr or Ba) electron density profiles at (0, 0), (b) B-site (Ti or Ru) electron density profiles at (0.5, 0.5), and (c) O-site electron density profiles at (0.5, 0) along the [001] direction.

**Figure 5 |** Out-of-plane lattice parameters of STO, bottom SRO, BTO, top SRO layers.

**References**


[1] H. Y. Hwang, Y. Iwasa, M. Kawasaki, B. Keimer, N. Nagaosa, Y. Yokura, Emergent Phenomena at Oxides Interfaces, Nat. Mater. 11, 103 (2012).

[2] J. Mannhart, D. G. Schlom, Oxides Interfaces-An Opportunity for Electronics, Science 327, 1607 (2010).

[3] A. K. Yadav, C. T. Nelson, S. L. Hsu, Z. Hong, J. D. Clarkson, C. M. Schelpüetz, A. R. Damodaran, P. Shafer, E. Arenholz, L. R. Dedon, D. Chen, a. Vishwanath, A. M. Minor, L. Q. Chen, J. F. Scott, L. W. Martin, R. Ramesh, Observation of Polar Vortices in Oxide Superlattices, Nature 530, 198 (2016).

[4] A. Ohtomo, H. Y. Hwang, A High-mobility Electron Gas at the $LaAlO_3/SrTiO_3$ Heterointerface, Nature 427, 423 (2004).

[5] J. Heber, Material Science : Enter The Oxides, Nature 459, 28 (2009).

[6] J. Chakhalian, A. J. Millis, J. Rondinelli, Wither the Oxide Interface, Nat. Mater. 11, 92-94 (2012)

[7] P. Zubko, S. Gariglio, M. Gavay, P. Ghosez, J. -M. Triscone, Interface Physics in Complex oxide Heterostructures, Annu, Rev. Condes. Matter Phys. 2, 141-165 (2011).

[8] M. Huijben, A. Brinkman, G. Koster, G. Rijnders, H. Hilgenkamp, D. H. A. Blank, Adv. Matter. 21, 1665 (2009).

[9] N. Reyren, S. Thiel, A. D. Caviglia, L. Fitting Kourkoutis, G. Hammerl, C. Richter, C. W. Schneider, T. Kopp, A. -S. Rüetschi, D. Jaccard, M. Gabay, D. A. Muller, J. -M. Triscone, J. Mannhart, Superconducting Interfaces Between Insulating Oxides, Science 317, 1196 – 1199 (2007).

[10] D. Xiao, W. Zhu, Y. Ran, N. Nagaosa, S. Okamoto, Interface Engineering of Quantum Hall Effects in Digital Transition Metal Oxide Heterostructures, Nat. Commun. 2. 596 - 598 (2011).

[11] M. Stengel, D. Vanderbilt, N. A. Spaldin, Enhancement of Ferroelectricity at Metal-oxide Interfaces, Nat. Materials. 8, 392-397 (2009).

[12] Yeong Jae Shin, Yoonkoo Kim, Sung-Jin Kang, Ho-Hyun Nahm, Pattukkannu Murugavel, Jeong Rae Kim, Myung Rae Cho, Lingfei Wang, Sang Mo Yang, Jong-Gul Yoon, Jin-Seok Chung,

Miyoung Kim, Hua Zhou, Seo Hyoung Chang, Tae Won Noh, Interface Control of Ferroelectricity in an $SrRuO_3$/$BaTiO_3$/$SrRuO_3$ Capacitor and its Critical Thickness, Adv. Matter. 29, 1602795 (2017).

[13] Yizhak Yacoby, Hua Zhou, Ron Pindak, and Ivan Božovic, Atomic-layer Synthesis and Imaging Uncover Broken Inversion Symmetry in $La_{2-x}Sr_xCuO_4$ films, Phys. Rev. B 87, 014108 (2013).

[14] D. D. Fong, C. Cionca, Y. Yacoby, G. B. Stephenson, J. A. Eastman, P. H. Fuoss, S. K. Streiffer, Carol Thompson, R. Clarke, R. Pindak, E. A. Stern, Direct Structural Determination in Ultrathin Ferroelectric Films by Analysis of Synchrotron X-ray Scattering Measurements, Phys. Rev. B 71, 144112 (2005).

[15] Hua Zhou, Anomalous of Expansion of the Copper-apical-oxygen Distance in Superconducting Cuprate Bilayers, Proc. Natl Acad. Sci. USA 107, 8103-8107 (2010).

[16] M. C. Wittels, F. A. Sherrill, Fast Neutron Effects in Tetragonal Barium Titanate, Journal of Applied Physics 28, 606-609 (1957).

[17] S. A. Howard, J. K. Yau, H. U. Anderson, Structural Characteristics of $Sr_{1-x}La_xTiO_{3+d}$ as a Function of Oxygen Partial Pressure at 1400°C, Journal of Applied Physics 65, 1492 – 1498 (1989).

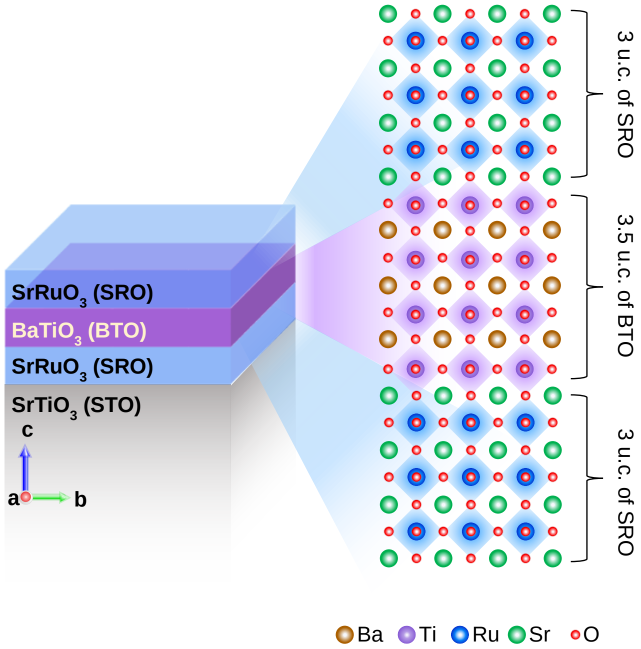


K. J. Lee *et al.*, Fig. 1.

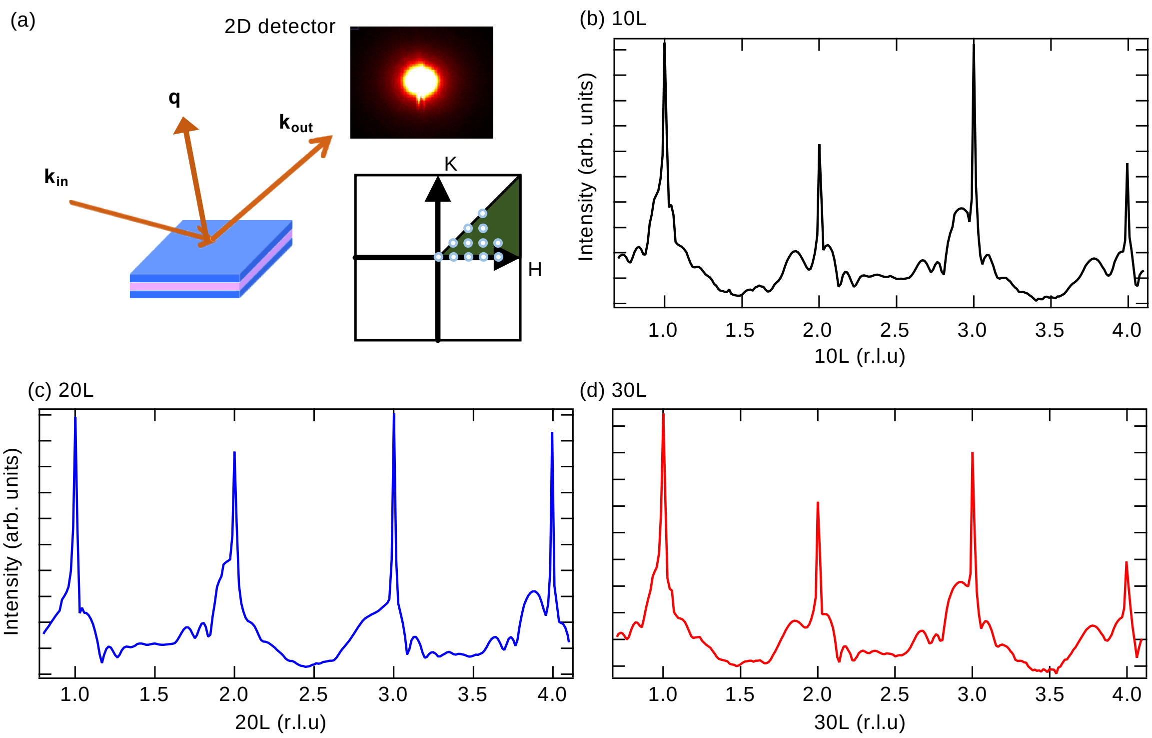


K. J. Lee *et al*., Fig. 2.

(a) (200) plane

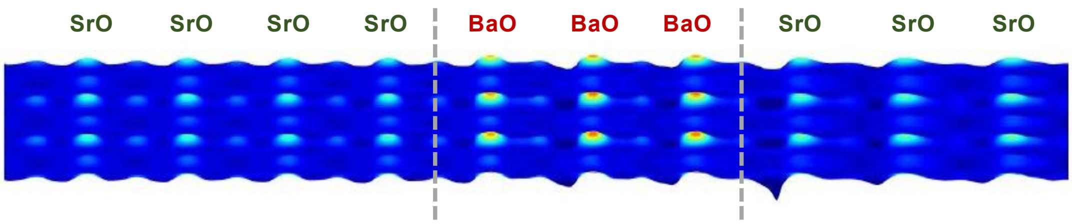


(b) B($O_2$)-site (001) plane

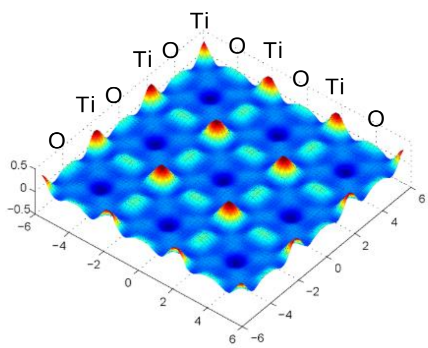

K. J. Lee *et al.*, Fig. 3.

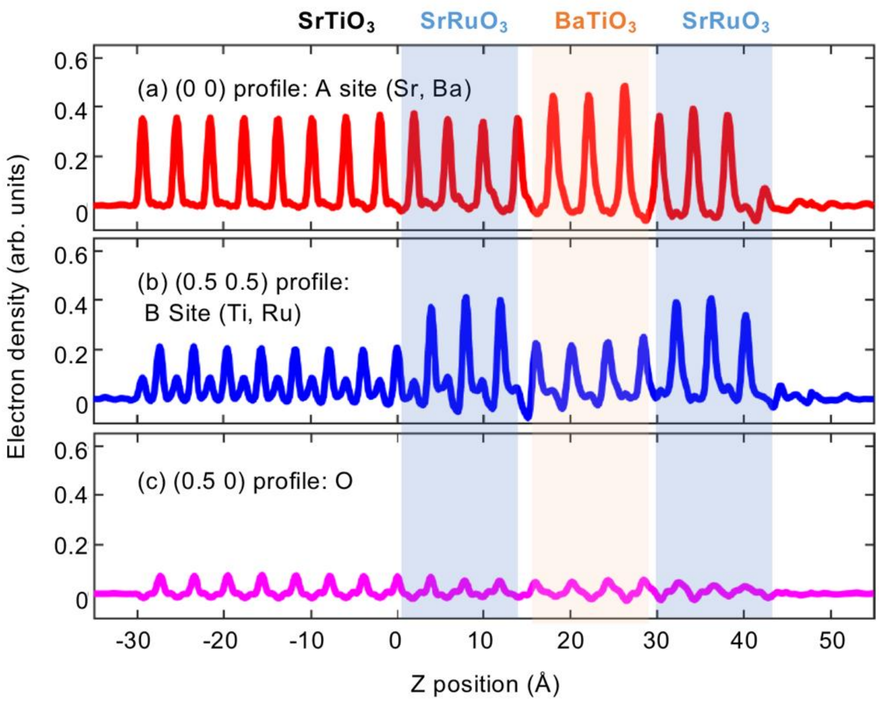

K. J. Lee *et al.*, Fig. 4.

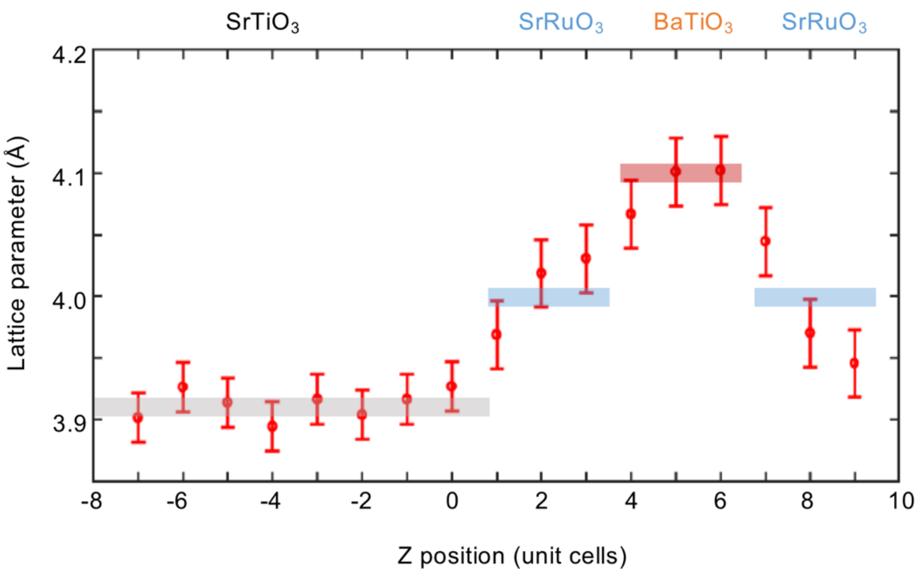

K. J. Lee *et al.*, Fig. 5.